THE STAR FORMATION NEWSLETTER No. 340 (#1-9)

塚越崇(NAOJ)

21 May 2021

1. **ALMA-IRDC: Dense gas mass distribution from cloud to core scales**
2. Fragmentation and kinematics in high-mass star formation: CORE-extension targeting two very young high-mass star-forming regions
3. SEDBYS: A Python-Based SED Builder for Young Stars
4. Magnetic fields and Star Formation around HII regions: The S235 complex
5. Unraveling the Inner Substructure of New Candidate Hub-Filament System in the HII Region G25.4NW
6. The Hi-GAL Compact Source Catalogue -- II. The 360° Catalogue of Clump Physical Properties
7. **Launching the Asymmetric Bipolar Jet of DO Tau**
8. Magnetic Fields in Massive Star-Forming Regions (MagMaR) I. Linear Polarized Imaging of the UCHII Region G5.89-0.39
9. Streaming Instability in a Global Patch Simulation of Protoplanetary Disks

ALMA-IRDC: Dense gas mass distribution from cloud to core scales A.T. Barnes et al.

ABSTRACT

Infrared dark clouds (IRDCs) are potential hosts of the elusive early phases of high-mass star formation (HMSF). Here we conduct an in-depth analysis of the fragmentation properties of a sample of 10 IRDCs, which have been highlighted as some of the best candidates to study HMSF within the Milky Way. To do so, we have obtained a set of large mosaics covering these IRDCs with ALMA at band 3 (or 3 mm). These observations have a high angular resolution ($\sim 3''$; ~ 0.05 pc), and high continuum and spectral line sensitivity (~ 0.15 mJy beam^{-1} and ~ 0.2 K per 0.1 km s^{-1} channel at the N_2H^+ $(1-0)$ transition). From the dust continuum emission, we identify 96 cores ranging from low- to high-mass ($M = 3.4 - 50.9 M_\odot$) that are gravitationally bound ($\alpha_{vir} = 0.3 - 1.3$) and which would require magnetic field strengths of $B = 0.3 - 1.0$ mG to be in virial equilibrium. We combine these results with a homogenised catalogue of literature cores to recover the hierarchical structure within these clouds over four orders of magnitude in spatial scale (0.01 pc – 10 pc). Using supplementary observations at an even higher angular resolution, we find that the smallest fragments (< 0.02 pc) within this hierarchy do not currently have the mass and/or the density required to form high-mass stars. Nonetheless, the new ALMA observations presented in this paper have facilitated the identification of 19 (6 quiescent and 13 star-forming) cores that retain >16 $M_\odot$ without further fragmentation. These high-mass cores contain trans-sonic non-thermal motions, are kinematically sub-virial, and require moderate magnetic field strengths for support against collapse. The identification of these potential sites of high-mass star formation represents a key step in allowing us to test the predictions from high-mass star and cluster formation theories.

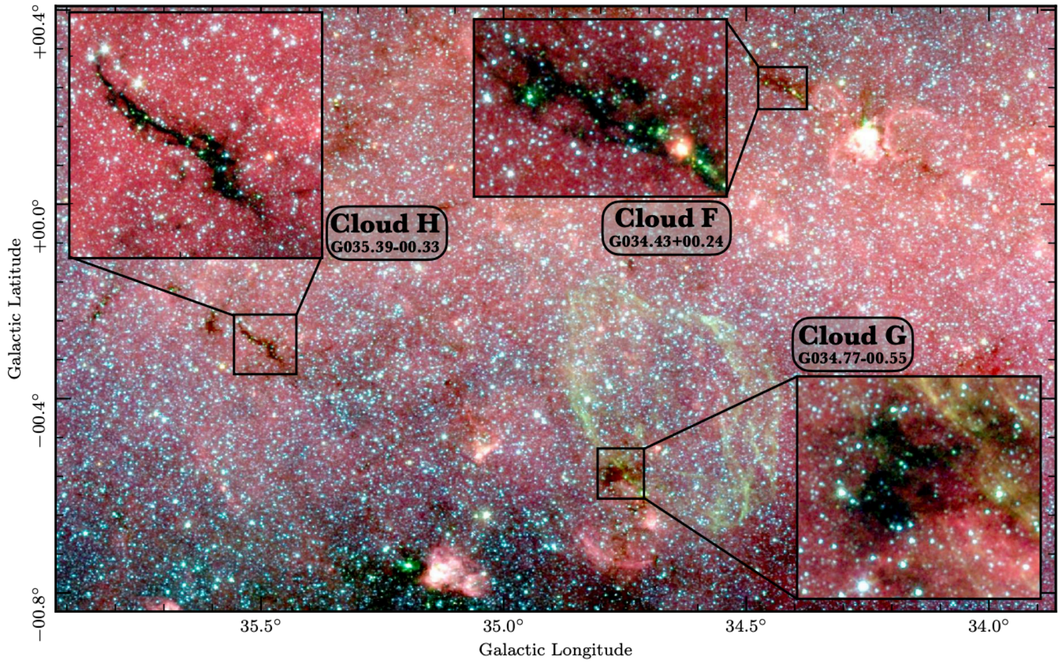

- 10個のIRDCのALMA 3mm連続波+N2H+(1-0)観測
- IRDCの階層構造の調査とHigh-mass star-forming core candidates探し

- 距離見積もり, IRデータ, 近傍,high-mass =>10 IRDCを選定
- ALMA Band3
  - 3mm連続波
  - N2H+(1-0)
    - Isolated hyperfineを使用
  - 12m+7m
  - Δθ=0.05-0.1pc
- Dendrogramによるコア同定(3mm cont.)
- N2H+による速度構造導出

Cloud	ID “G(longitude)(latitude)”	v_{sys} km s^{-1}	D_{cl} pc	$R_{eff,cl}$ pc	M_{cl} $M_\odot$	σ_{cl} km s^{-1}	$\alpha_{vir,cl}$ -	$T_{dust,cl}$ K	$\sigma_{NT,cl}$ km s^{-1}	$\mathcal{M}_{NT,cl}$ -	n_c #
Cloud A	G018.82-00.28	59-69	4800	10.4	18500.0	2.04	1.4	18.3	2.0	7.9	8
Cloud B	G019.27+00.07	22-32	2400	2.71	2200.0	1.6	2.2	17.8	1.6	6.3	10
Cloud C	G028.37+00.07	73-83	5000	15.4	53200.0	3.72	2.4	17.7	3.7	14.8	16
Cloud D	G028.53-00.25	81-91	5700	16.9	74300.0	1.85	0.5	16.9	1.8	7.5	16
Cloud E	G028.67+00.13	75-85	5100	11.5	28700.0	4.32	1.1	19.1	4.3	16.5	4
Cloud F	G034.43+00.24	52-62	3700.0	3.5	4460.0	3.62	1.3	20.0	3.6	13.5	20
Cloud G	G034.77-00.55	35-45	2900	3.06	3300.0	3.28	4.7	19.8	3.3	12.3	0
Cloud H	G035.39-00.33	38-48	2900	9.69	16700.0	2.03	0.7	19.5	2.0	7.6	10
Cloud I	G038.95-00.47	38-48	2700	3.73	2700.0	1.65	1.2	18.0	1.6	6.4	9
Cloud J	G053.11+00.05	17-27	1800	0.755	200.0	0.96	1.5	19.0	0.9	3.5	3

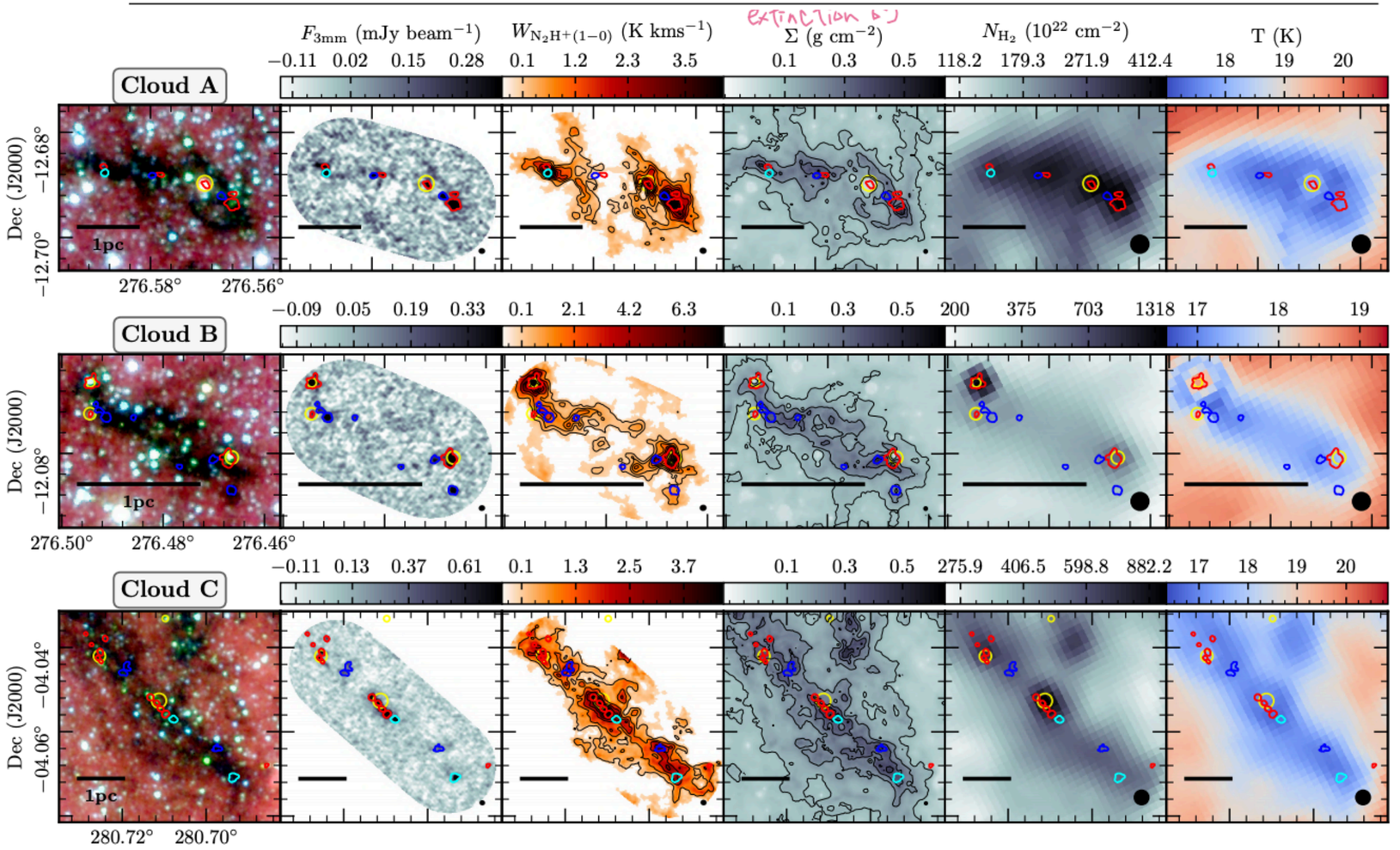

- コア構造のproperties

N2H+速度構造同定

- 複数成分フィット
- コア分布に対応する成分を抽出
- 線幅からnon-thermal成分を算出

  ->Mach number

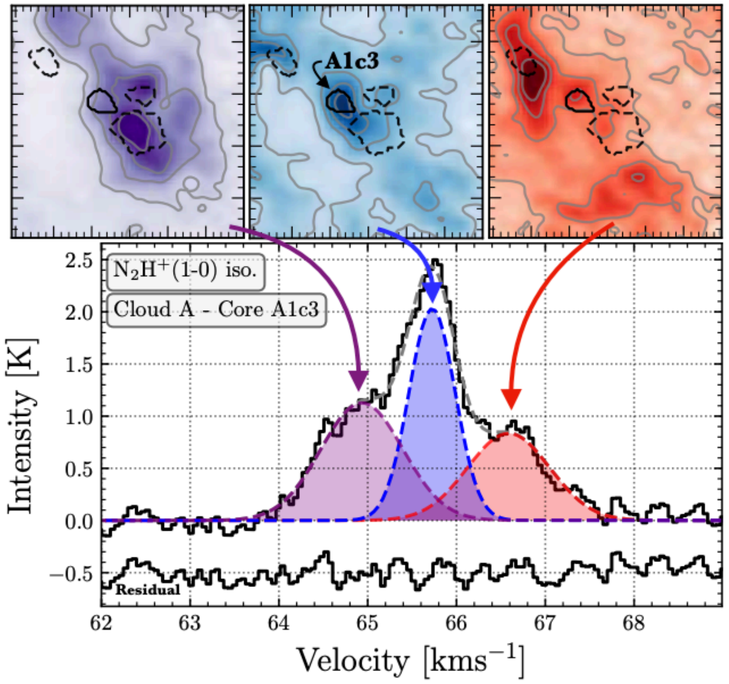

IR-3mm 質量比較

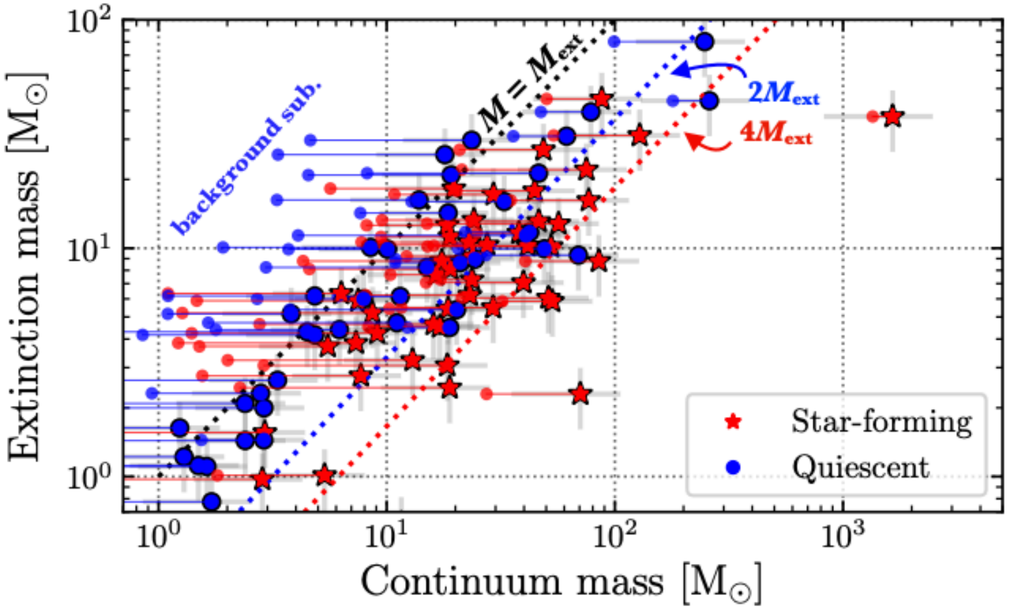

同定コアの物理量

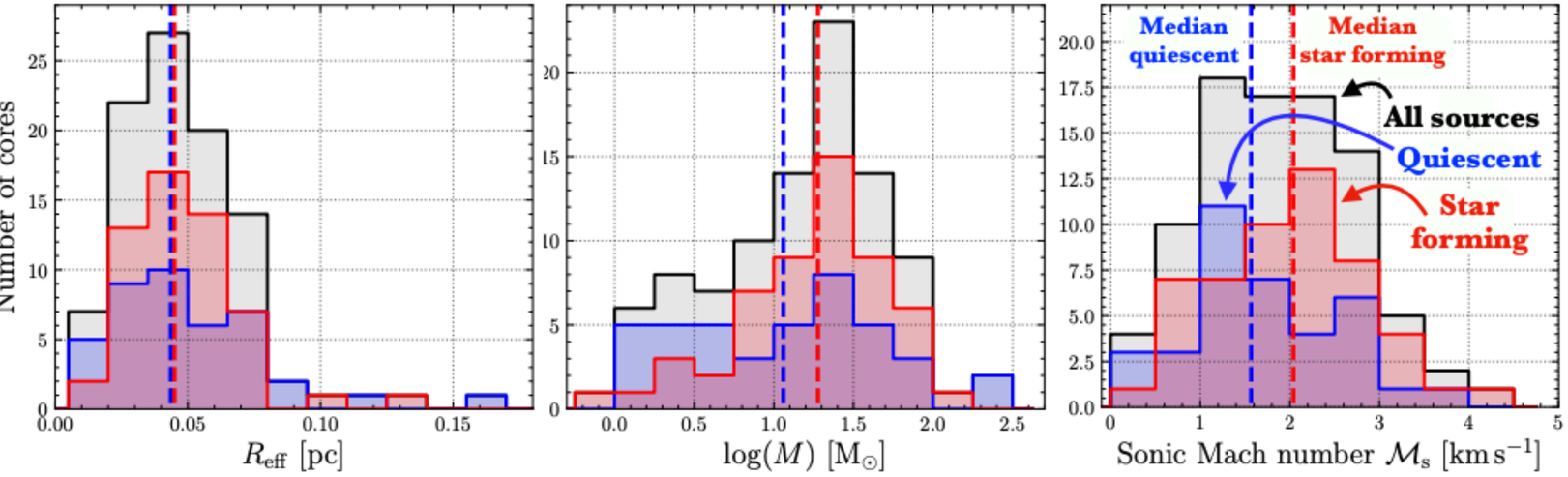

コアの安定性

- 熱+乱流だけではX
- Reasonableな磁場強度によるサポートがあれば安定

- 他空間構造との比較

0.1-1pc構造: Clump(R06), 0.01-0.1pc: Core(This work, H16), smallest: Core-fragments(L18,H17)

質量-サイズ関係

- Clump->Coreで密度1~2桁上昇
- Clump~Coreスケールではl81よりKP10 relation
  - 導出スケールや質量計算の違いなど

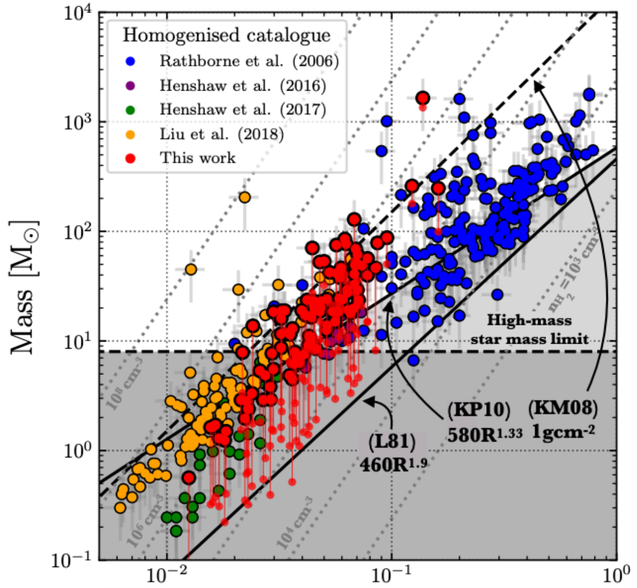

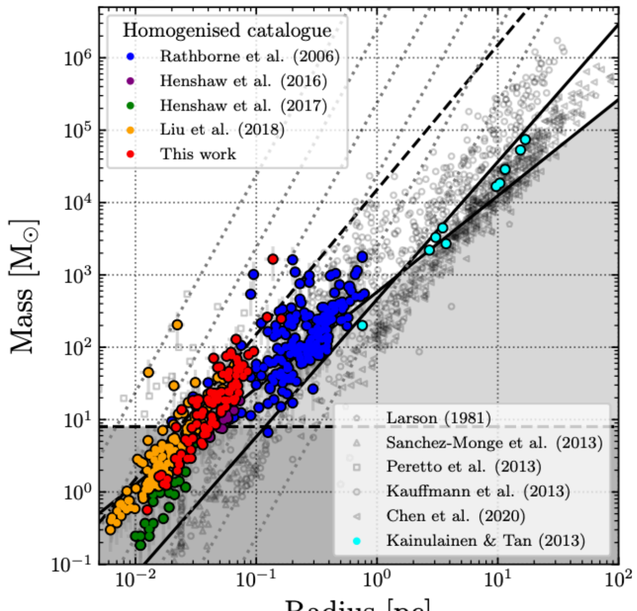

速度構造

- いくつかはsub-thermal
- 多くのコアはvirialized

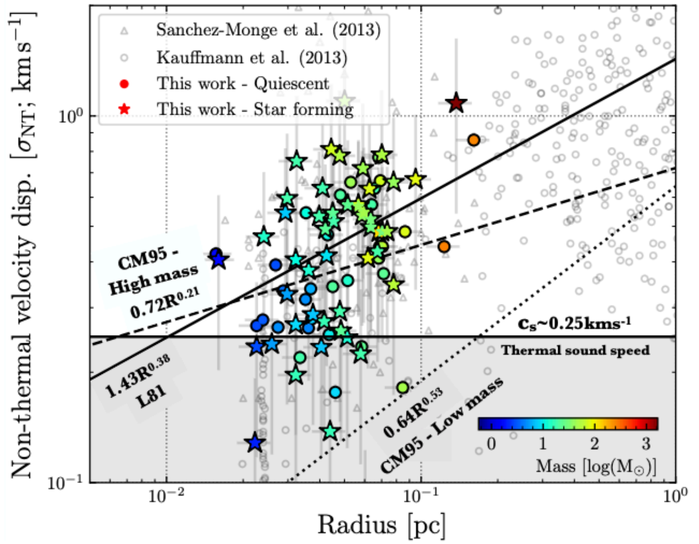

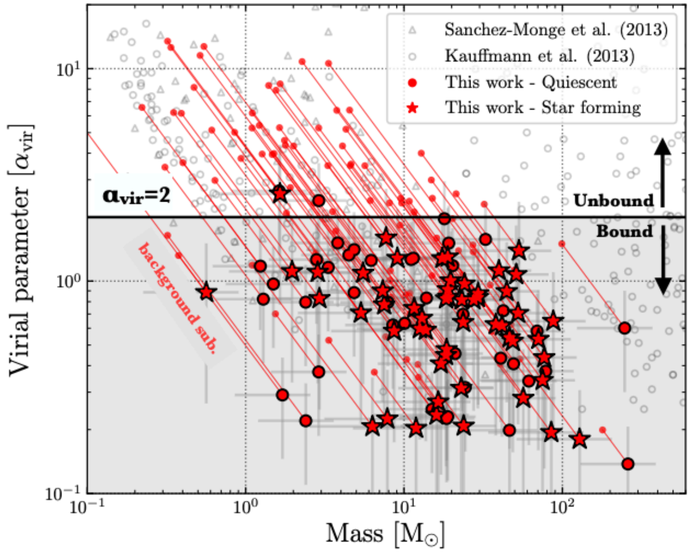

- (IRDC→)Clump→Core→Core-fragmentsの階層構造
  - 空間構造が一致するもの
  - Core-fragmentsがない/1つだけ
  - Core-fragmentsが複数であればhigh-massを含むもの

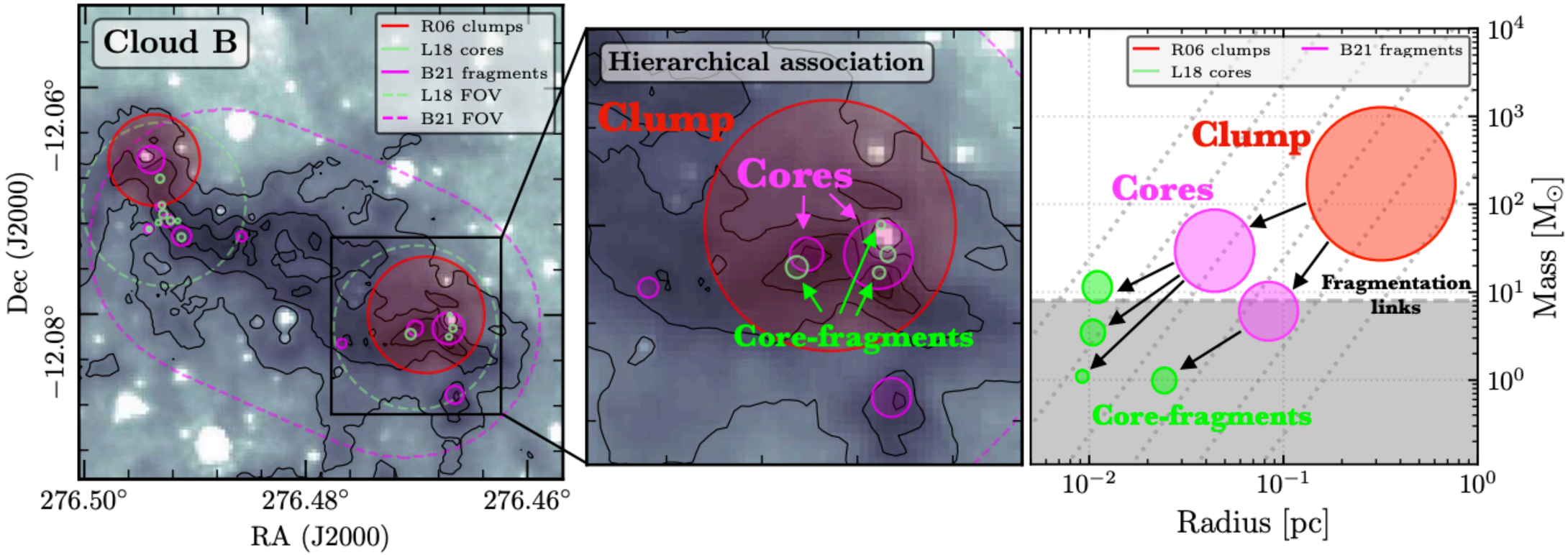

→19個の構造をID

- Quiescent core (6個)
  - Trans-sonic non-thermal motion
  - Sub-viral
  - 976μGの磁場がないとcollapseする
  - High-mass star-forming coreの良いサンプル
- Star-forming (13個)
  - Quiescent coreより高密度
  - 線幅,ビリアル比もQuiescentより大
- コアサイズはcore-accretion theory[McKee&Tan2003]の予想と broadly comparable

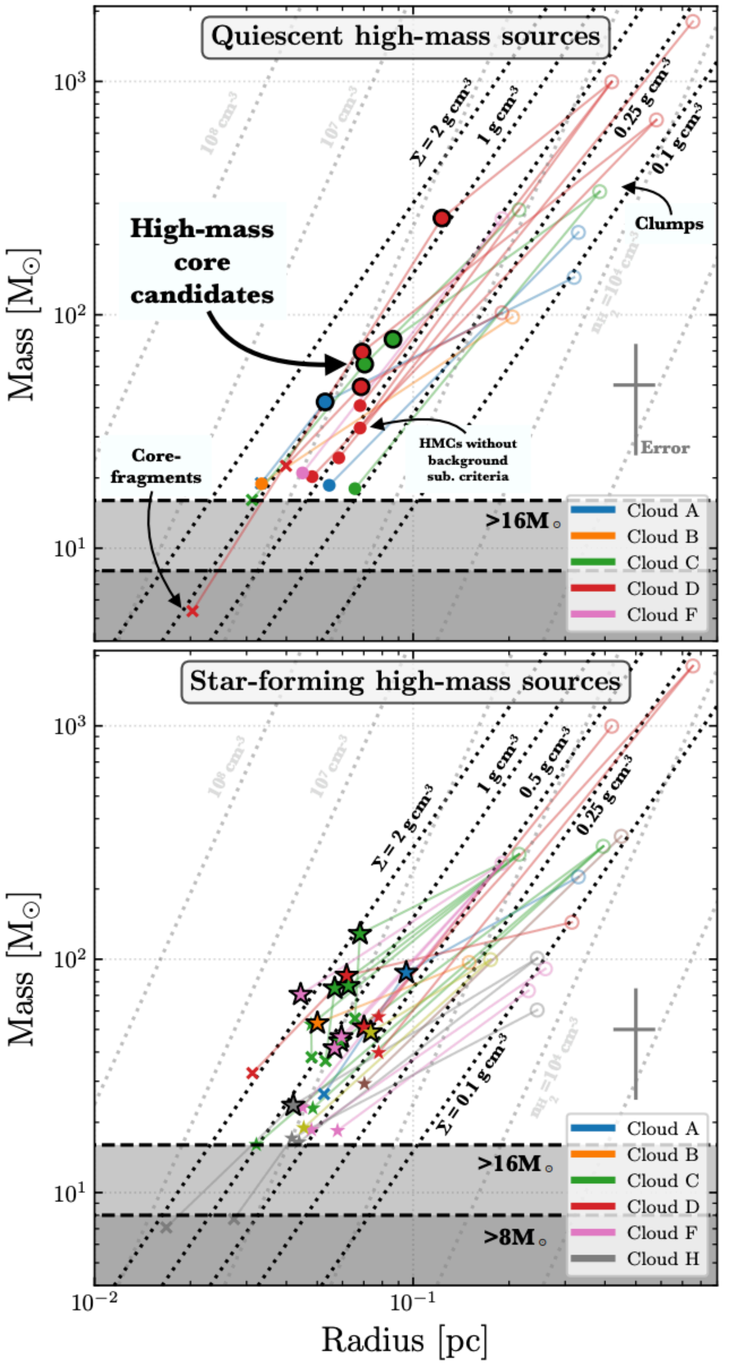

- Cloudとの相関
- 温度↗でジーンズ長↗
  - 3D構造を考える必要あり
- コア個数と線幅関係
  - Turbulentな雲が複数のコアを産む
    - 質量/半径も大

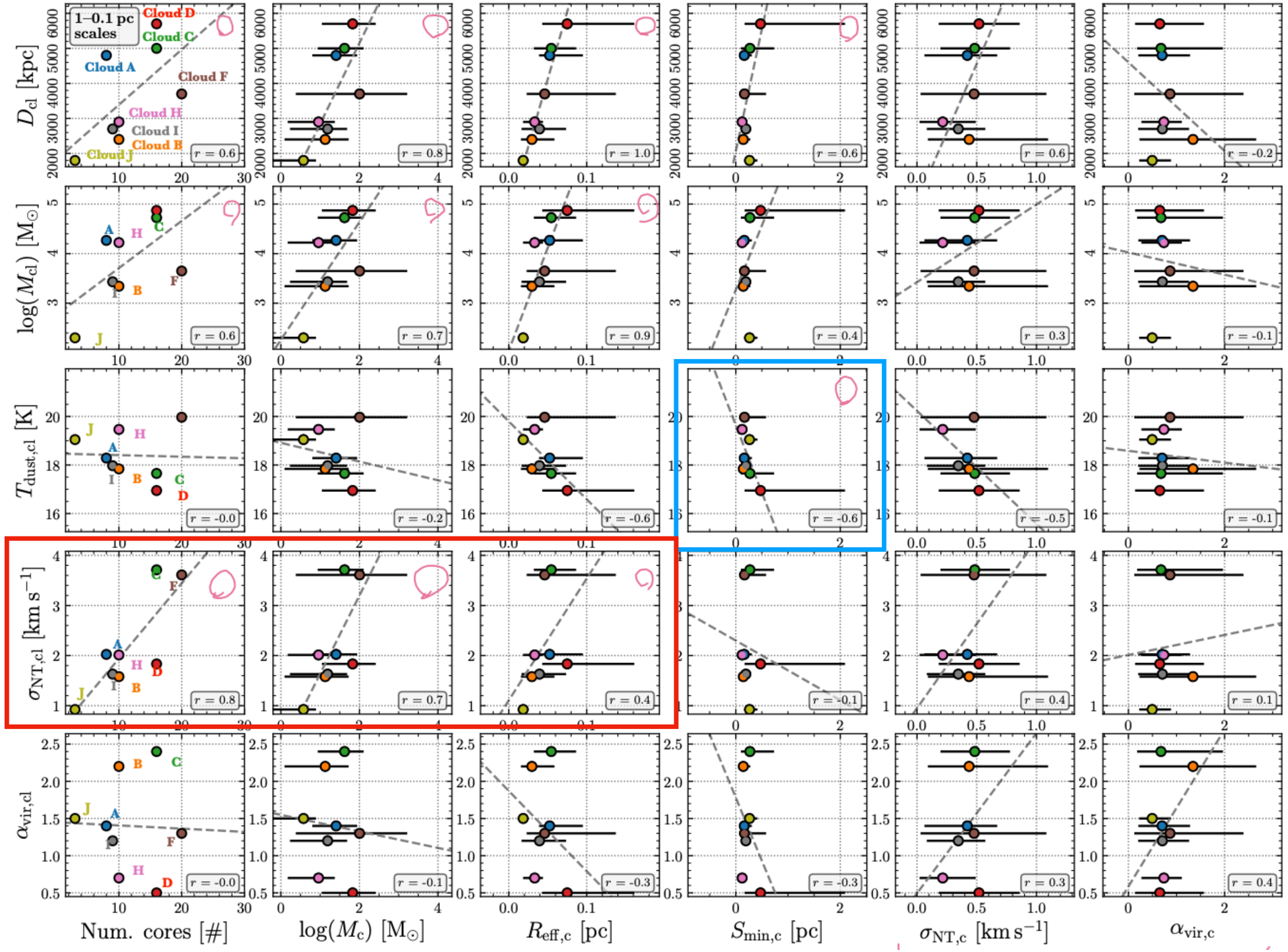

Launching the asymmetric bipolar jet of DO Tau
J. Erkal et al.

ABSTRACT

Context. The role of bipolar jets in the formation of stars, and in particular how they are launched, is still not well understood.
Aims. We probe the protostellar jet launching mechanism, via high resolution observations of the near-IR [Fe II]λ1.53,1.64 μm emission lines.
Methods. We consider the case of the bipolar jet from Classical T Tauri star, DO Tau, and investigate the jet morphology and kinematics close to the star (within 140 au), using AO-assisted IFU observations from GEMINI/NIFS.
Results. We find that the brighter, blue-shifted jet is collimated very quickly after it is launched. This early collimation requires the presence of magnetic fields. We confirm velocity asymmetries between the two lobes of the bipolar jet, and also confirm no time variability in the asymmetry over a 20 year interval. This sustained asymmetry is in accordance with recent simulations of magnetised disk-winds. We examine the data for signatures of jet rotation. We report an upper limit on differences in radial velocity of 6.3 and 8.7 km s^{-1} for the blue and red-shifted jets, respectively. Interpreting this as an upper limit on jet rotation implies that any steady, axisymmetric magneto-centrifugal model of jet launching is constrained to a launch radius in the disk-plane of $r_0 < 0.5$ and 0.3 au for the blue and red-shifted jets, respectively. This supports an X-wind or narrow disk-wind model. However, the result pertains only to the observed high velocity [Fe II] emission, and does not rule out a wider flow launched from a wider radius. We report detection of small amplitude jet axis wiggling in both lobes. We rule out orbital motion of the jet source as the cause. Precession can better account for the observations but requires double the precession angle, and a different phase for the counter-jet. Such non-solid body precession could arise from an inclined massive Jupiter companion, or a warping instability induced by launching a magnetic disk-wind.
Conclusions. Overall, our observations are consistent with an origin of the DO Tau jets from the inner regions of the disk.

- DOTauのjetを高解像度NIR観測
- 非対称速度構造やwiglling構造などを検出

- Jetの駆動は未解明
  - Stellar photosphereに刺さる磁場駆動
  - Star-Disk磁場駆動のwind
  - 広い領域にわたるDisk wind
- →高解像度観測でjetの根元を見る

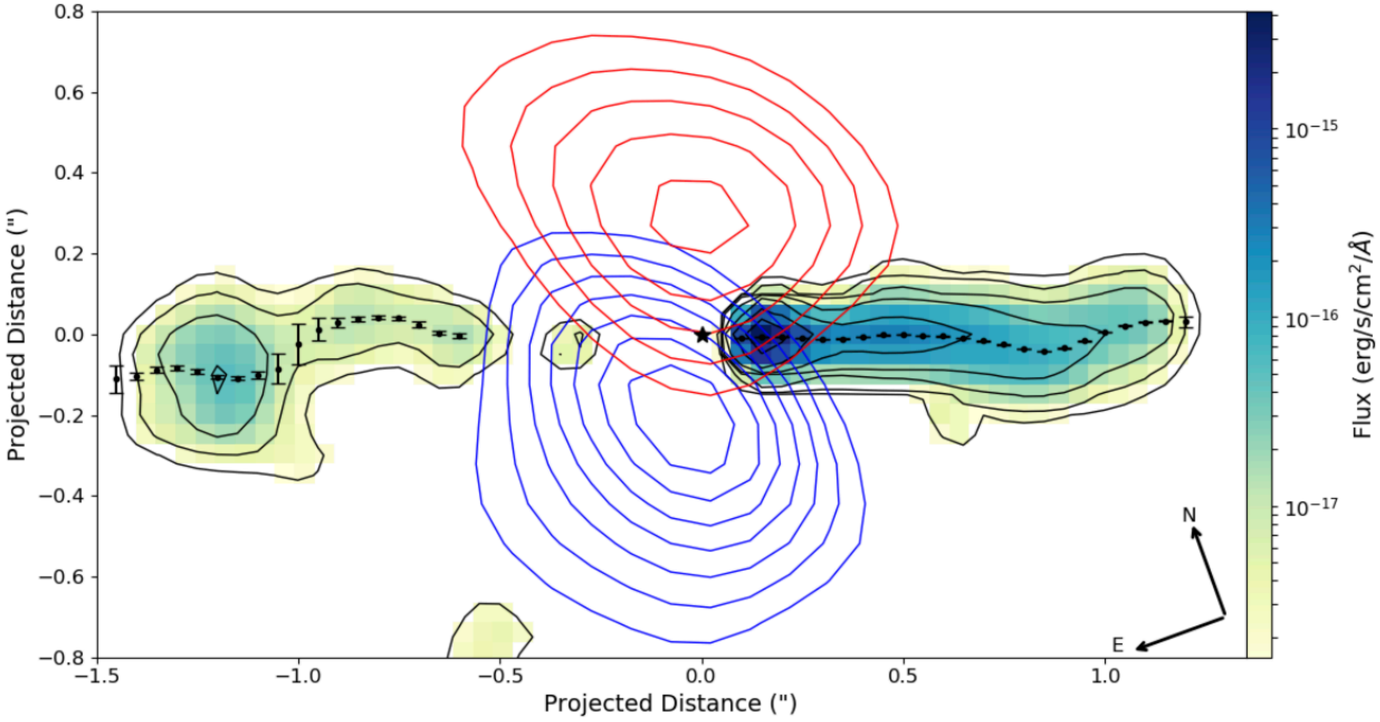

- Gemini-North NIFS
  - AO assisted H-band obs.
  - [Fe II] at NIR (1.53, 1.60, 1.64μm)
    - dv=56km/s
  - 0.15-0.175” FWHM
- ALMA C18O(2-1)
  - 円盤回転に垂直
  - Collimated
  - 構造/強度非対称
    - [blue] SNR高, 星近傍まで見える
    - [red] SNR低, 星近傍は円盤減光で見えない
  - Wiggling
    - Semi-opening angle=1.3° at 90au

- 速度非対称
  - 文献とconsistent→no time variability
  - 駆動メカニズムに起因しているはず
    - blue, redで同程度のcollimation
    - 速度変化なし

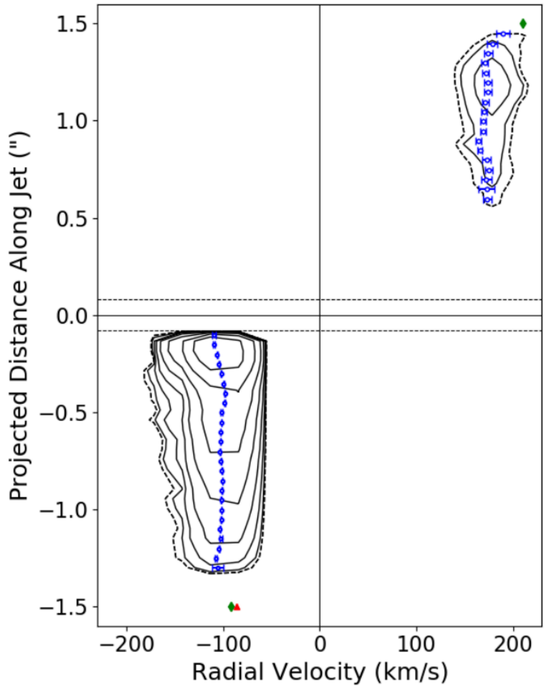

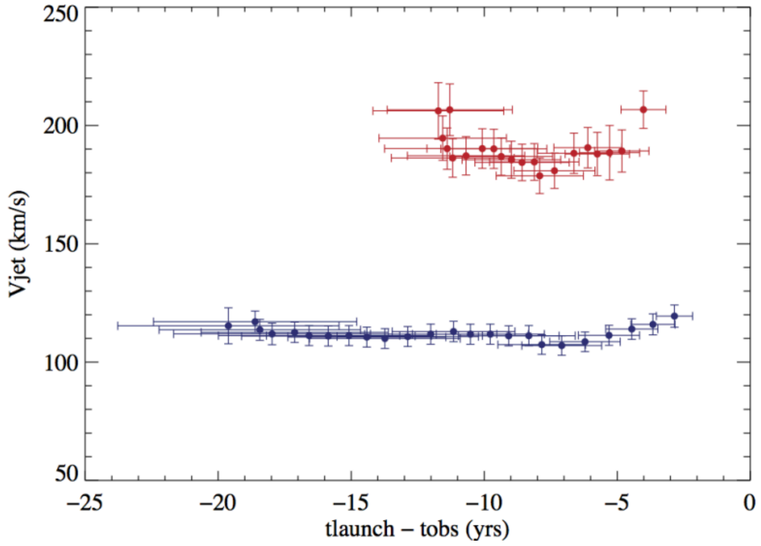

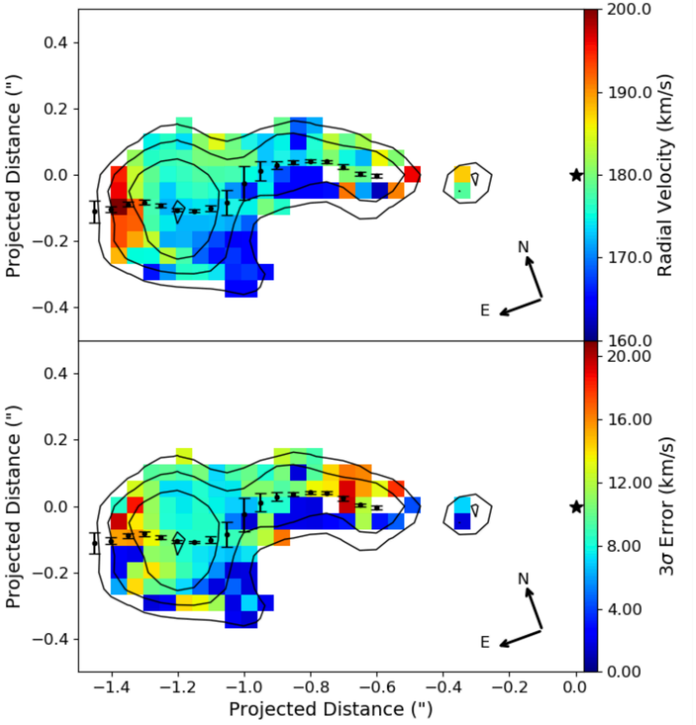

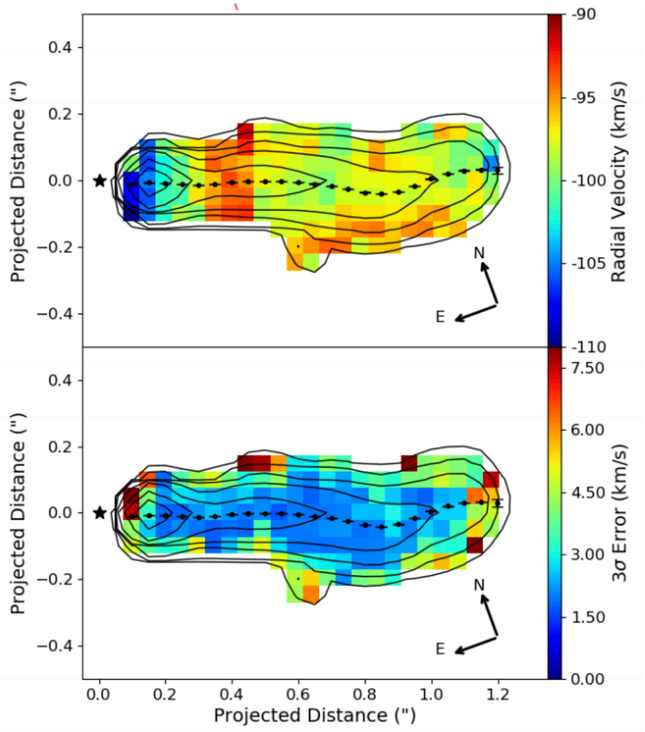

- ショック構造
  - 急激な速度変化は見られず
  - Blue側0.4″あたりで系統的な速度変化

    →弱いshock front?
    - Knotなどは見られない

- Electron number densityとmass flux

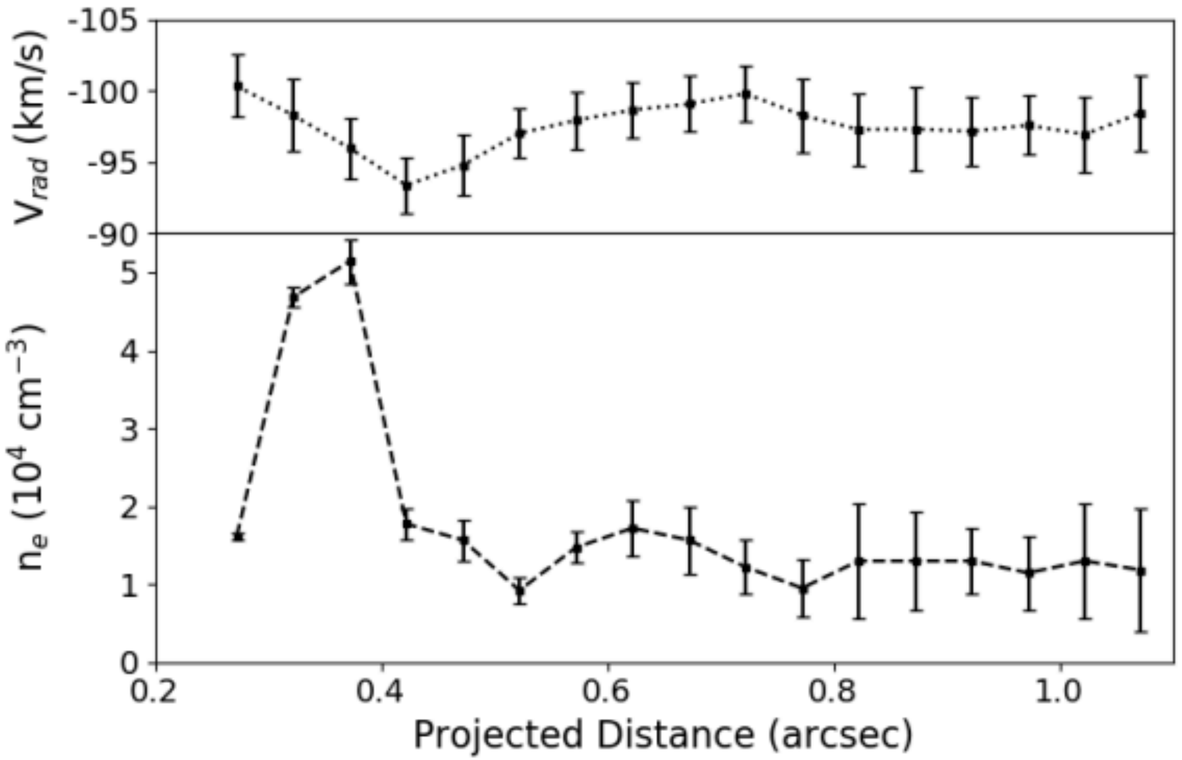

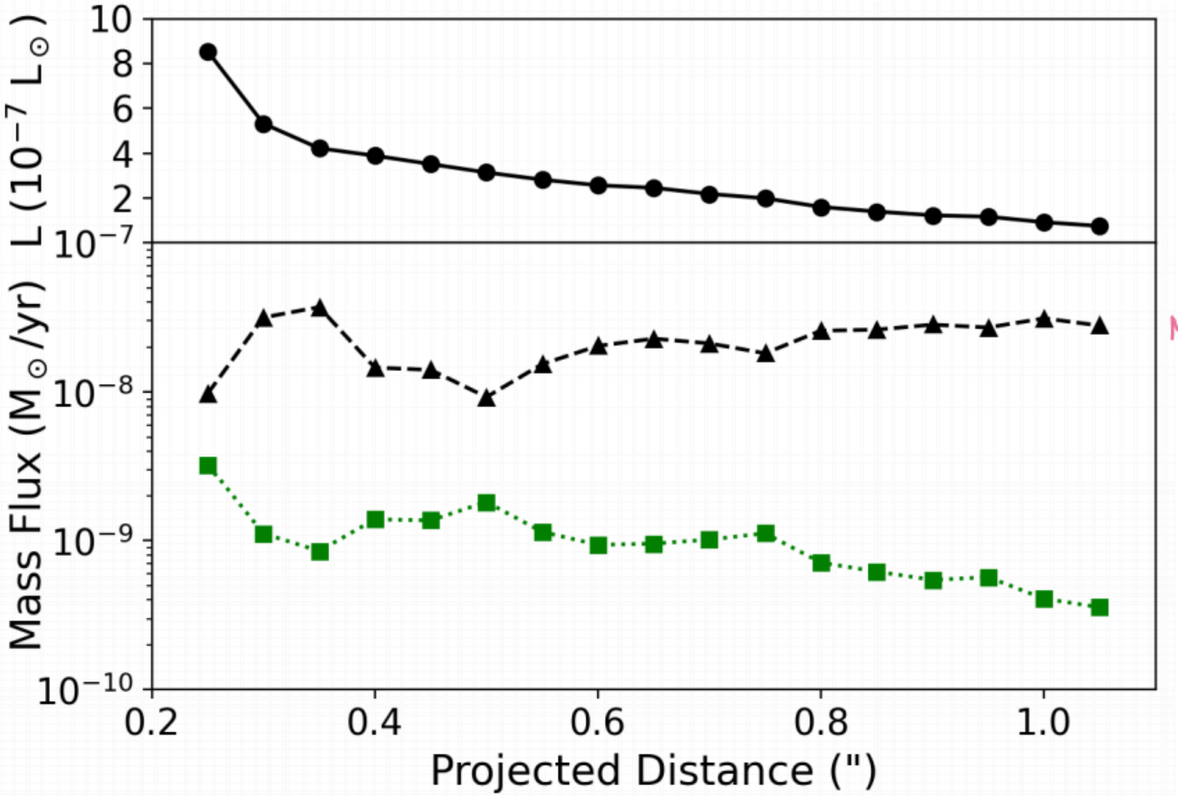

- [Fe II] 1.53μm/1.64μmから算出
- 低解像度の文献値と整合

- 2手法で算出(upper/lower limitに対応)
  - 均一なnHを仮定する方法
  - [FeII]強度とn_eを用いる方法
- fluctuationはn_eとχ_eが縮退

- Origin of bipolar jet
  - Launching radius r_0の見積もり
    - r_0^b<0.5au, r_0^r<0.3au
      同一のr_0の可能性があるが、速度非対称
      なども考えると異なるr_0の可能性もある
  - Magnetic lever arm parameter
    $\lambda \simeq (r_A/r_0)^2$の見積もり
    - λ^b<6.25, λ^r<11
    - MHD disk wind起源の可能性もある
  - 駆動メカニズム自体は区別できないが、
    high-velocity jetは0.5au以内の円盤領域で
    駆動している

- Origin of wiggling
  - Orbital scenario
  - Precession scenario
    - Star-disk (misaligned) interaction
    - 惑星でもいい
      - 6-12MJ at 0.1-0.15au
  - Precession by magnetic torque
    - 可能性あり

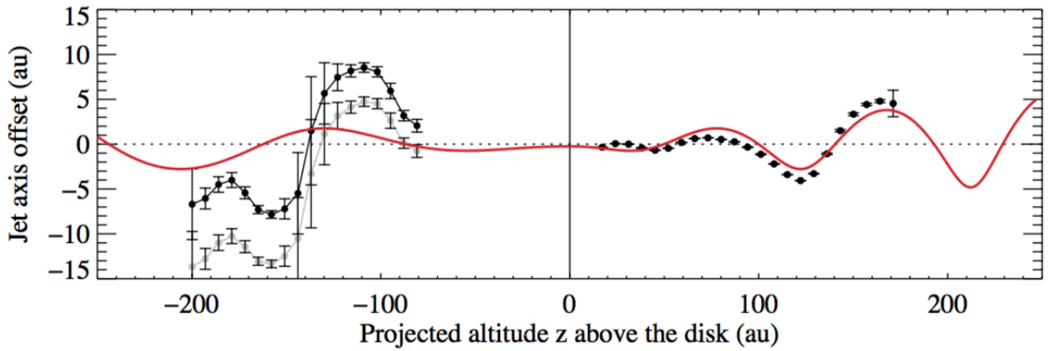

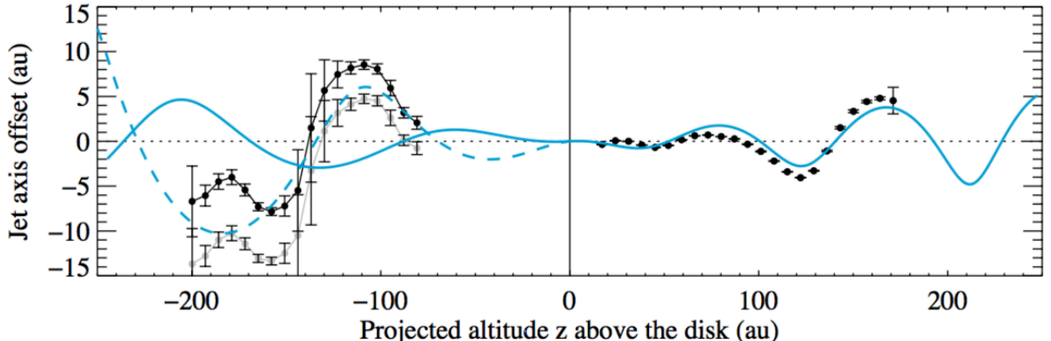

Fragmentation and kinematics in high-mass star formation: CORE-extension targeting two very young high-mass star-forming regions

H. Beuther et al.

Context. The formation of high-mass star-forming regions from their parental gas cloud and the subsequent fragmentation processes lie at the heart of star formation research.

Aims. We aim to study the dynamical and fragmentation properties at very early evolutionary stages of high-mass star formation.

Methods. Employing the NOrthern Extended Millimeter Array (NOEMA) and the IRAM 30 m telescope, we observed two young high-mass star-forming regions, ISOSS22478 and ISOSS23053, in the 1.3 mm continuum and spectral line emission at a high angular resolution (~0.8″).

Results. We resolved 29 cores that are mostly located along filament-like structures. Depending on the temperature assumption, these cores follow a mass-size relation of approximately $M \propto r^{2.0\pm0.3}$, corresponding to constant mean column densities. However, with different temperature assumptions, a steeper mass-size relation up to $M \propto r^{3.0\pm0.2}$, which would be more likely to correspond to constant mean volume densities, cannot be ruled out. The correlation of the core masses with their nearest neighbor separations is consistent with thermal Jeans fragmentation. We found hardly any core separations at the spatial resolution limit, indicating that the data resolve the large-scale fragmentation well. Although the kinematics of the two regions appear very different at first sight – multiple velocity components along filaments in ISOSS22478 versus a steep velocity gradient of more than 50 km s^{-1} pc^{-1} in ISOSS23053 – the findings can all be explained within the framework of a dynamical cloud collapse scenario.

Conclusions. While our data are consistent with a dynamical cloud collapse scenario and subsequent thermal Jeans fragmentation, the importance of additional environmental properties, such as the magnetization of the gas or external shocks triggering converging gas flows, is nonetheless not as well constrained and would require future investigation.

SEDBYS: A python-based SED Builder for Young Stars Claire L Davies

Abstract

Spectral energy distributions (SEDs) are useful primary and complementary tools in the analysis of observations of young stars. However, the process of collating, inspecting, and flux-converting archival photometry and spectroscopy to build spectral energy distributions for young stars is time-consuming. Here, I present SEDBYS (Spectral Energy Distribution Builder for Young Stars), a python-based repository of command-line tools built to (i) query online photometric and spectroscopic catalogs and a distributed database of archival photometry, (ii) use a look-up table of zero points to flux-convert the acquired data, (iii) enable interactive visual inspection of the SED and (iv) handle book-keeping to collate references in bibTeX format. The code is distributed via git and is equipped with additional tools to enable users to add existing or forthcoming catalogs to the list of sources queried, ensuring the longevity of SEDBYS as a tool for the star formation community.

Magnetic fields and Star Formation around HII regions: The S235 complex
R. Devaraj et al.

Magnetic fields are ubiquitous and essential in star formation. In particular, their role in regulating formation of stars across diverse environments like H II regions needs to be well understood. In this study, we present magnetic field properties towards the S235 complex using near-infrared (NIR) *H*-band polarimetric observations, obtained with the Mimir and POLICAN instruments. We selected 375 background stars in the field through combination of *Gaia* distances and extinctions from NIR colors. The plane-of-sky (POS) magnetic field orientations inferred from starlight polarization angles reveal a curved morphology tracing the spherical shell of the H II region. The large-scale magnetic field traced by *Planck* is parallel to the Galactic plane. We identified 11 dense clumps using 1.1 mm dust emission, with masses between $33 - 525\,M_\odot$. The clump averaged POS magnetic field strengths were estimated to be between $36 - 121\,\mu$G, with a mean of $\sim 65\,\mu$G. The mass-to-flux ratios for the clumps are found to be sub-critical with turbulent Alfvén Mach numbers less than 1, indicating a strongly magnetized region. The clumps show scaling of magnetic field strength vs density with a power-law index of 0.52 ± 0.07, similar to ambipolar diffusion models. Our results indicate the S235 complex is a region where stellar feedback triggers new stars and the magnetic fields regulate the rate of new star formation.

Unraveling the inner substructure of new candidate hub-filament system in the HII region G25.4NW

L. K. Dewangan

ABSTRACT

We present multi-scale and multi-wavelength data of the Galactic H II region G25.4-0.14 (hereafter G25.4NW, distance ~5.7 kpc). The SHARC-II 350 μm continuum map displays a hub-filament configuration containing five parsec scale filaments and a central compact hub. Through the 5 GHz radio continuum map, four ionized clumps (i.e., Ia–Id) are identified toward the central hub, and are powered by massive OB-stars. The *Herschel* temperature map depicts the warm dust emission (i.e., T_d ~23–39 K) toward the hub. High resolution Atacama Large Millimeter/submillimeter Array (ALMA) 1.3 mm continuum map (resolution ~0.″82 × 0.″58) reveals three cores (c1–c3; mass ~80–130 $M_\odot$) toward the ionized clumps Ia, and another one (c4; mass ~70 $M_\odot$) toward the ionized clump Ib. A compact near-infrared (NIR) emission feature (extent ~0.2 pc) is investigated toward the ionized clump Ia excited by an O8V-type star, and contains at least three embedded K-band stars. In the direction of the ionized clump Ia, the ALMA map also shows an elongated feature (extent ~0.2 pc) hosting the cores c1–c3. All these findings together illustrate the existence of a small cluster of massive stars in the central hub. Considering the detection of the hub-filament morphology and the spatial locations of the mm cores, a global non-isotropic collapse (GNIC) scenario appears to be applicable in G25.4NW, which includes the basic ingredients of the global hierarchical collapse and clump-fed accretion models. Overall, the GNIC scenario explains the birth of massive stars in G25.4NW.

The Hi-GAL compact source catalogue – II. The 360° catalogue of clump physical properties
D. Elia et al.

ABSTRACT

We present the 360° catalogue of physical properties of Hi-GAL compact sources, detected between 70 and 500 μm. This release not only completes the analogous catalogue previously produced by the Hi-GAL collaboration for $-71^\circ \lesssim \ell \lesssim 67^\circ$, but also meaningfully improves it thanks to a new set of heliocentric distances, 120808 in total. About a third of the 150223 entries are located in the newly added portion of the Galactic plane. A first classification based on detection at 70 μm as a signature of ongoing star-forming activity distinguishes between protostellar sources (23 per cent of the total) and starless sources, with the latter further classified as gravitationally bound (pre-stellar) or unbound. The integral of the spectral energy distribution, including ancillary photometry from $\lambda = 21$ to 1100 μm, gives the source luminosity and other bolometric quantities, while a modified black body fitted to data for $\lambda \geq 160$ μm yields mass and temperature. All tabulated clump properties are then derived using photometry and heliocentric distance, where possible. Statistics of these quantities are discussed with respect to both source Galactic location and evolutionary stage. No strong differences in the distributions of evolutionary indicators are found between the inner and outer Galaxy. However, masses and densities in the inner Galaxy are on average significantly larger, resulting in a higher number of clumps that are candidates to host massive star formation. Median behaviour of distance-independent parameters tracing source evolutionary status is examined as a function of the Galactocentric radius, showing no clear evidence of correlation with spiral arm positions.

Magnetic Fields in Massive Star-Forming Regions (MagMaR) I. Linear Polarized Imaging of the UCHII Region G5.89-0.39

M. Fernández-López et al.

We report 1.2 mm polarized continuum emission observations carried out with the Atacama Large Millimeter/submillimeter Array (ALMA) toward the high-mass star formation region G5.89–0.39. The observations show a prominent 0.2 pc north-south filamentary structure. The UCHII in G5.89–0.39 breaks the filament in two pieces. Its millimeter emission shows a dusty belt with a mass of 55-115 $M_\odot$ and 4,500 au in radius, surrounding an inner part comprising mostly ionized gas with a dust emission only accounting about 30% of the total millimeter emission. We also found a lattice of convex arches which may be produced by dragged dust and gas from the explosive dispersal event involving the O5 Feldt's star. The north-south filament has a mass between 300-600 $M_\odot$ and harbours a cluster of about 20 millimeter envelopes with a median size and mass of 1700 au and 1.5 $M_\odot$, respectively, some of which are already forming protostars.

We interpret the polarized emission in the filament as mainly coming from magnetically aligned dust grains. The polarization fraction is $\sim$ 4.4% in the filaments and 2.1% at the shell. The magnetic fields are along the North Filament and perpendicular to the South Filament. In the Central Shell, the magnetic fields are roughly radial in a ring surrounding the dusty belt between 4,500 and 7,500 au, similar to the pattern recently found in the surroundings of Orion BN/KL. This may be an independent observational signpost of explosive dispersal outflows and should be further investigated in other regions.

Streaming instability in a global patch simulation of protoplanetary disks Mario Flock et al.

Aims. In the recent years, sub/mm observations of protoplanetary disks have discovered an incredible diversity of substructures in the dust emission. An important result was the finding that dust grains of mm size are embedded in very thin dusty disks. This implies that the dust mass fraction in the midplane becomes comparable to the gas, increasing the importance of the interaction between the two components there.
Methods. We address this problem by means of numerical 2.5D simulations in order to study the gas and dust interaction in fully global stratified disks. To this purpose, we employ the recently developed dust grain module in the PLUTO code. Our model focuses on a typical T Tauri disk model, simulating a short patch of the disk at 10 au which includes grains of constant Stokes number of $St = 0.01$ and $St = 0.1$, corresponding to grains with sizes of 0.9 cm and 0.9 mm, respectively, for the given disk model.
Results. By injecting a constant pebble flux at the outer domain, the system reaches a quasi steady state of turbulence and dust concentrations driven by the streaming instability. For our given setup and using resolutions up to 2500 cells per scale height we resolve the streaming instability, leading to local dust clumping and concentrations. Our results show dust density values of around 10-100 times the gas density with a steady state pebble flux between 3.5×10^{-4} and $2.5 \times 10^{-3} M_{\rm Earth}/year$ for the models with $St = 0.01$ and $St = 0.1$.
Conclusions. The grain size and pebble flux for model $St = 0.01$ compares well with dust evolution models of the first million years of disk evolution. For those grains the scatter opacity dominates the extinction coefficient at mm wavelengths. These types of global dust and gas simulations are a promising tool for studies of the gas and dust evolution at pressure bumps in protoplanetary disks.